Simulated Supercells in Non-tornadic and Tornadic VORTEX2 Environments: Storm-scale Differences

Brice E. Coffer* and Matthew D. Parker

Department of Marine, Earth, and Atmospheric Sciences, North Carolina State University, Raleigh, NC

1. Introduction

Since the Verification of the Origins of Rotation in Tornadoes Experiment (VORTEX; Rasmussen et al. 1994) in the mid-1990s, considerable progress has been made regarding our understanding of how lower tropospheric profiles of temperature, humidity, and winds favor non-tornadic versus tornadic supercells (e.g. Rasmussen and Blanchard 1998, Markowski et al. 2003, Thompson et al. 2003, 2007, Craven and Brooks 2004). However, it is still unclear how these environmental differences, especially the wind profile, affect the in-storm processes that lead to tornadogenesis.

To begin to address this gap in the knowledge base, the second VORTEX field campaign (VORTEX2; Wurman et al. 2012) collected numerous near-supercell soundings, in conjunction with other observational platforms, in order to assess the near-storm variability and to further understand the relationship between the environment and tornadoes. To identify reoccurring differences between non-tornadic and tornadic supercell environments, Parker (2014) generated composite environments (from 134 soundings) of the 12 best sampled VORTEX2 supercells; this included 7 tornadic and 5 non-tornadic supercells. The "storm-following" sounding network regularly launched from 4 locations (Parker 2014): distant-inflow (~70-100 km from the storm's updraft), near-inflow (~30-40 km from the storm's updraft), and the forward and rear flanks outflow regions of the active supercells. The near-inflow composite soundings (Figs. 1, 2) displayed the most interesting differences between the non-tornadic and tornadic supercells.

**Corresponding author address*: Brice Coffer, North Carolina State University, Campus Box 8208, Raleigh, NC, 27615-8208; *email*: becoffer@ncsu.edu

Both near-inflow composite soundings are seemingly favorable for tornadoes, with the convective available potential energy (CAPE) values greater than 2000 J/kg and storm-relative helicity (SRH) near 300 m^2/s^2 in the effective inflow layer (Figs. 1, 2). Each profile has a significant tornado parameter that is above the climatological median for EF3+ tornadoes (Thompson et al. 2003)[1]. The most noticeable difference is in the low-level wind profile, specifically the amount of streamwise horizontal vorticity in the lowest 500 m.

Using observed proximity soundings (instead of RUC model derived soundings typically used in climatological datasets), Esterheld and Guiliano (2008) showed that SRH integrated over the 0 – 500 m layer demonstrated the highest discrimination between non-tornadic and tornadic supercells, compared to deeper layers. Additionally, the angle between the 0 – 500 m shear vector and the 10 m storm-relative inflow vector (referred to as the "critical angle") was most commonly near 90 degrees for the significantly tornadic supercells (i.e. purely streamwise), while for the non-tornadic supercells, the critical angle was much more frequently near 110 degrees.

In the VORTEX2 dataset, the 0 – 500 m SRH is twice as high in tornadic composite compared to the non-tornadic (158 vs. 80 m^2/s^2, respectively), and just as in Esterheld and Guiliano (2008), the critical angle is approximately 90 degrees for the tornadic environment, whereas the non-tornadic environment has a critical angle of 132 degrees (Figs. 1, 2). This indicates that there is significant streamwise horizontal vorticity in tornadic environment.

[1] As noted in Parker (2014), common forecasting parameters, such as low-level shear and lifted condensation level (LCL), were enhanced in the near-inflow environment, thus the soundings used herein are not a perfect comparison with the RUC-generated proximity soundings.

Increased SRH in the lowest few hundred meters may promote stronger dynamic lifting by the supercell's mesocyclone near the surface, increasing the likelihood of tornadogenesis (Markowski et al. 2012, Markowski and Richardson 2014a; Coffer and Parker 2015). Alternatively, the orientation of the low-level winds may alter the interaction between the cold pool and shear, leading to an unfavorable, backward-tilted updraft orientation (Nowotarski and Jensen 2014).

The purpose of this paper is to explore contrasting storm-scale characteristics in full-physics supercell simulations initialized with the pair of VORTEX2 composite environments. Details regarding the methods are described in Section 2. Results and interpretation from the simulations are offered in Section 3, while a summary of the main conclusions and avenues for future work are presented in Section 4.

2. Methods

a. Model configuration

To examine potentially relevant differences to tornadogenesis between the non-tornadic and tornadic VORTEX2 composite environments, supercells simulations were conducted using release 17 of the Bryan Cloud Model 1 ("CM1"; Bryan and Fritsch 2002). These storms were simulated for 2 h on a 200 x 200 x 18 km^3, horizontally homogeneous domain initialized using the near-inflow composite VORTEX2 soundings from Parker (2014) discussed previously. The horizontal grid spacing is 125 m within a 100 km x 100 km inner domain centered on the right-moving supercell and gradually increases to 3.875 km at the edges of the domain (Wilhelmson and Chen 1982). The lowest scalar grid level is at 10 m, and from there, the vertical grid spacing stretches from 20 m in the lowest 300 m to 280 m at 12 km, allowing for 31 levels in the lowest kilometer. The compressible, non-hydrostatic equations were discretized on an Arakawa C grid (Arakawa and Lamb 1977) and integrated forward using a time step of 0.6 s, with eight split time steps for the acoustic modes (Klemp and Wilhelmson 1978). A fifth-order advection scheme, utilizing high-order weighted essentially non-oscillatory finite differencing, is used with no additional artificial diffusion (Shu 2003, Wicker and Skamarock 2002).

A six-category, fully double-moment bulk microphysics scheme from the National Severe Storms Laboratory that explicitly predicts the variable densities of hail and graupel is used (Ziegler 1985; Mansell et al. 2010), with the shape parameters ($\propto_{g,hl}$) of 0.0 and 2.0, respectively. A high concentration of cloud condensation nuclei was chosen to represent the base-state (1.5 x 10^9), representative of a typical continental air mass found in the VORTEX2 operational domain. Convection was initiated using the updraft nudging technique described by Naylor et al. (2012). The nudging is defined in a spheroid with 15-km horizontal radius and a 2.5-km vertical radius centered at z = 2.5 km (near the LFC) during the first 1200 s of the simulations ($\propto$ = 0.5 s^{-1}, w_{max} = 15 m/s; notation as in Naylor et al. 2012). The subgrid-scale turbulence is controlled by a 1.5 order turbulence kinetic energy closure scheme similar to Deardorff (1980), with separate horizontal and vertical turbulence coefficients and a zero flux boundary condition. Open, radiative lateral boundary conditions were employed (Klemp and Wilhelmson 1978), while the upper-boundary has a rigid, free-slip boundary condition, with a Rayleigh damping sponge applied above 14 km. The bottom-boundary condition is "semi-slip" and is described in more detail below.

b. Semi-slip bottom boundary condition

Idealized simulations of supercell thunderstorms have almost exclusively been conducted using free-slip bottom boundary conditions. In these simulations, baroclinic generation of vorticity near the surface produces intense, tornado-like vortices. However, recently, frictional generation of vorticity has been investigated and at times been found to be a dominant contributor to the vorticity budget (e.g. Schenkman et al. 2014, Markowski and Richardson 2014c). In a first step towards incorporating surface drag into idealized, full-physics supercell simulations, we have applied a constant drag exchange coefficient (C_d) of 0.001. This value is similar to the C_d calculated from the composite VORTEX2 *rear-flank outflow* sounding using the revised surface layer scheme in WRF (Jimenez et al. 2012) and sample C_d values given in Stull (1988; pg. 267). The value of C_d from the composite near-inflow sounding was approximately 0.005, similar to those reported in Frame and Markowski 2010 and Nowotarski et al. 2015, however the rear-flank

outflow is the main area of interest for vorticity generation and tornadogenesis; thus a smaller C_d value (characteristic of a profile with higher stability) was preferred. Certainly, future work with these simulations will need to investigate the effect of increasing values of C_d, especially when addressing the role of surface drag in the development of near-ground rotation, as opposed to the storm-scale differences discussed herein. Regardless, including surface drag (even if small) represents a more physically consistent framework for the bottom boundary condition compared to the habitually employed free-slip assumption.

Coriolis force was applied to the perturbation winds in order to minimize the impact of the friction on the base-state environmental wind profile. This introduces a force that opposes friction once a new steady state is acquired and is equivalent to assuming that the initial wind profile is in geostrophic balance. The Coriolis parameter *(f)* was set to 10^{-4}, a typical mid-latitude value. This method was preferred over others tested; including nudging back to the base-state and applying a fictitious 'PGF-like' acceleration in the low-levels, due to its simplicity of implementation (built-in namelist option in CM1) and the fact that Coriolis acceleration represents a physical process that is present in the real atmosphere. In our tests, the preservation of the low-level wind profile by the Coriolis wind is more noticeable for idealized quarter-turn and semicircle hodographs. A nice characteristic of real-data soundings is the near-surface wind observation is much closer to zero. This confines the modification of the low-level wind profile to the lowest 300 m, but even in these observed wind profiles, there is an advantage of minimizing changes to the far field profiles by using the Coriolis force on the perturbation winds.

Since the Coriolis force operates on timescales of several hours, each environmental profile was first simulated in a small-domain simulation with the same model configuration described in Section 2a (except for periodic lateral boundaries and no convection initialization). After roughly four hours, the wind profile in the lowest two hundred meters arrives at quasi-steady state. Each of the horizontally homogeneous supercell simulations discussed herein are initialized using a sounding extracted at this time (t = 4 h). The wind profile remains nearly steady-state in the far inflow environment throughout simulation[2].

3. Results

a. Storm evolution

Both simulations develop supercellular convection (an expected yet encouraging result) within the first 45 min[3] of initialization (Fig. 3 a,d) and exhibit common supercell features, including a forward-flank precipitation region, a well-defined rear-flank outflow, and a "hook echo" reflectivity structure (an indication of a low-level mesocyclone; LLM). The non-tornadic supercell's LLM cycles frequently, where the LLM is advected towards the rear of the storm (Fig 3 b,c). Within the 30 min window plotted in Figure 4, the non-tornadic supercell has four distinct hook echoes and LLMs. In contrast, the tornadic supercell has a persistent and strong LLM (Fig 3 d-f). A nearly steady LLM would seemingly be a more favorable configuration for tornadogenesis.

Both storms possess a strong updraft in the mid-levels (4 – 5 km), with velocities exceeding 40 m/s (Fig. 4). The low-level updraft (0 – 3 km) in the tornadic supercell is much stronger; velocities greater than 50 m/s are occasionally present as low as 500 m. Since both environments have similar values of CAPE, these differences in the updraft velocity are likely due to dynamical influences.

The contrasting low-level updrafts alter the development of surface vortices. The non-tornadic supercell only produces shallow vortices that are more transient in nature, failing to be maintained over a significant period of time (Fig. 5). Compared to the tornadic supercell, several intense, long-lasting vortices develop (Fig. 5). One near-surface vortex in

[2] The far inflow wind profile does not evolve exactly as in the small-domain simulation due to gravity waves produced by the convection and their subsequent interaction with the open, radiative lateral boundaries, among other convective processes.

[3] The relatively quick spin-up of supercellular convection is due to the updraft-nudging initialization method, which initiates the model with a developed updraft rather than an updraft developing from a thermal perturbation or prescribed convergence.

particular, at t = 60 min, has a peak intensity of 0.8 s^{-1} and lasts for approximately 20 minutes.

b. Superposition of updraft and surface vorticity

To further explore differences between the two supercells, time composites following the low-level updraft were created for the 15 minutes during the failed genesis in the non-tornadic supercell and the 15 minutes leading up to the most intense near-surface vortex in the tornadic supercell (see "time composite" labels in Fig. 5). In the non-tornadic supercell, the main updraft is several kilometers ahead of the precipitation and overall weaker (Fig. 6a). The tornadic supercell has a stronger updraft directly overlapping the hook echo (Fig. 6d). Both simulations produce surface circulations; however the non-tornadic supercell's circulation is behind the updraft, nearer to the precipitation (Fig. 6 b,e). Without being superimposed under the low-level updraft, the surface vorticity that does develop in the non-tornadic supercell is not being stretched into a deep, intense vortex.

The cold outflow is not much stronger in either simulation. The orientation of the "storm-relative" cold pool is different due to low-level winds mostly from the east in the non-tornadic case and mostly from the southeast in the tornadic case. Although both cold pools have similar potential temperature deficits, the gradient between the warm inflows and the cold outflows is sharper in the non-tornadic supercell. Considering this gradient and that the updraft is far ahead of the surface circulation, the non-tornadic supercell has many characteristics of an outflow-dominated supercell, which has long been surmised to be unfavorable for tornadogenesis.

c. Near-surface vortex-genesis, maintenance, and decay in the tornadic supercell

During the 15 minutes prior to near-surface vortexgenesis in the tornadic supercell, the low-level mesocyclone dramatically ramps up. The core of the updraft begins to extend towards lower levels, with maximum velocities at 1 km increasing from 20 to 50 m/s (Fig. 4), and the mesocyclone aloft rapidly intensifies (Fig. 7a -c). There is a failed near-surface vortex attempt approximately 5 minutes prior to vortexgenesis, and then the vortex spins up at the surface and lasts for almost 20 minutes (Fig 7d-f). Near the conclusion of the near-surface vortex, a second near-surface vortex develops and then both dissipate as cold air shunts the vortices away from main mesocyclone.

The intensification of the low-level updraft prior to near-surface vortex development is caused by an increase in the dynamic vertical perturbation pressure gradient acceleration (VPPGA). This induces stronger stretching at low-levels, the final requirement in the tornadogenesis processes. The low-level dynamic lifting increases over 300% in the 15 minutes prior to vortexgenesis (t = 60 min; Fig. 8). Preliminary work identifying parcels that end up in the LLM shows that many more LLM parcels traverse the forward flank during this intensification phase (not shown). This suggests that the updraft is possibly strengthening due to the updraft tilting enhanced horizontal vorticity baroclinically generated along the forward flank temperature gradient. The non-tornadic supercell also has increases in the VPPGA during its failed genesis period (t = 60-75 min), but it is not as strong (Fig. 8) nor in the vicinity of the surface circulation (similar to the low-level updraft in Fig. 6a,b).

Interestingly, as the updraft is intensifying a precipitation cell develops in the inflow region near the hook echo (Fig. 3d, Fig. 7b) and merges with the forward flank precipitation. Visually, this would likely look like precipitation curtains (PCs) developing near the rain-free base of the supercell. PCs could be a manifestation of the rapidly intensifying low-level updraft and could be of use to the warning process, although future work would need to identify these features in observations and compare their relation to tornadogenesis.

d. Baroclinic versus frictional generation of vorticity

Finally, we will briefly address the question of baroclinic versus frictional generation of vorticity. In this simulation, a vortex sheet develops in the forward flank (Fig 9a); vortex sheets have been identified in developing supercells in both observations and simulations (e.g. Beck and Weiss 2013, Markowski et al. 2014b). The vortex sheet rotates cyclonically around the intensifying mesocyclone, and then ends up being oriented north-south and feeds high vorticity parcels into the near-

surface vortex throughout its duration (Fig 9b,c). This has recently been termed a "river of vorticity" (Dahl et al. 2014; Parker and Dahl 2015). During the course of this process, the vortex sheet and eventually the vorticity river are associated with positive/negative couplets of vertical vorticity and along a temperature gradient (Fig 9 d-e). Qualitatively this suggests that baroclinic generation of vorticity is still important, even when the simulation features surface drag. However, much more rigorous analysis is needed, including vortex lines and vorticity budgets along trajectories.

4. Preliminary Conclusions

While our understanding of environments that favor tornadic versus non-tornadic storms has increased in recent years, it is still unclear how these factors influence within-storm processes. In the present study, we have begun to investigate how reoccurring differences between non-tornadic and tornadic environments observed during VORTEX2 result in supercells with contrasting characteristics in full-physics simulations. Our simulations using the composite VORTEX2 near-inflow soundings show the following:

1. The non-tornadic supercell has an unsteady LLM, cycling frequently. On the other hand, the tornadic supercell has a persistent LLM.
2. The low-level updraft is much stronger in the tornadic supercell. This leads to much stronger stretching of vorticity and results in long-lived, deep vortices, compared to shallow, transient vortices in the non-tornadic supercell.
3. The updraft in the non-tornadic supercell is several kilometers ahead of the precipitation, and while both supercells produce surface vorticity, the vorticity in the non-tornadic supercell is not superimposed underneath under the low-level updraft. Perhaps this is due to the sharp gradient between inflow and colder outflow, resulting in a supercell that resembles an "outflow-dominated" storm.
4. Preceding the most intense near-surface vortexgenesis in the tornadic supercell, there is a rapid intensification in the low-level updraft over 15 minutes. The updraft increase is accompanied by strengthening of the mesocyclone and an attendant increase in the dynamic vertical perturbation pressure gradient acceleration. The near-surface vortex dissipates as the low-level dynamic lifting decreases and a strong pulse of cold outflow overtakes the vortex.
5. Parcels feeding into the near-surface vortex during the genesis and maintenance periods are associated with couplets of positive/negative vertical vorticity along a temperature gradient. Qualitatively, it appears the baroclinity is still meaningful in near-surface vortex development in simulations with surface drag.

Future work will compare frequency distributions of storm storm-scale quantities of interest (e.g. updraft velocity, vertical vorticity, potential temperature perturbations, hydrometeor mixing ratios, etc.) to complement the maximum time-height plots (similar to Kumjian et al 2015). Furthermore, several scientific questions still need to be fully elucidated, including the failure point of the non-tornadic supercell, the importance of the 0 – 500 m SRH versus other environmental ingredients, the rapid updraft intensification in the tornadic supercell (and its interplay with the PCs and the forward flank vortex sheet rotating around the mesocyclone), and more quantitative analysis of the contribution of baroclinity versus surface drag (and the influence of C_d on storm evolution). Work is also underway to incorporate a data assimilation technique into CM1. Once complete, the tornadic supercell could be assimilated into the non-tornadic environment to determine if wind profile is most influential in storm development or whether it is actively favoring near-surface vortexgenesis. Finally, as of now, the simulations are with the VORTEX2 composite soundings as-is. It would be interesting to conduct a parameter space study systematically varying the low- and mid-level wind profile for a controlled hypothesis test.

Acknowledgements. NSF Grants AGS-1156123 and AGS-1359709, George Bryan for his ongoing support of CM1, and current/past members of the NCSU Convective Storms group.

REFERENCES

Arakawa, A., and V. Lamb, 1977: Computational design of the basic dynamical processes in the UCLA general

circulation model. General Circulation Models of the Atmosphere: Methods in Computational Physics, J. Chang, Ed., Vol. 17, Academic Press, 174–264.

Beck, J., and C. Weiss, 2013: An Assessment of Low-Level Baroclinity and Vorticity within a Simulated Supercell. *Mon. Wea. Rev.*, **141**, 649–669.

Bryan, G. H., and J. M. Fritsch, 2002: A benchmark simulation for moist nonhydrostatic numerical models. *Mon. Wea. Rev*., **130**, 2917–2928.

Coffer, B. and Matthew D. Parker, 2015: Impacts of Increasing Low-Level Shear on Supercells during the Early Evening Transition. *Mon. Wea. Rev.*, **143**, 1945–1969.

Craven, J. P., and H. E. Brooks, 2004: Baseline climatology of sounding derived parameters associated with deep, moist convection. *Nat. Wea. Digest*, **28**,13-24.

Dahl J., Matthew D. Parker, and Louis J. Wicker, 2014: Imported and Storm-Generated Near-Ground Vertical Vorticity in a Simulated Supercell. *J. Atmos. Sci.*, **71**, 3027–3051.

Deardorff, J. W., 1980: Stratocumulus-capped mixed layer derived from a three-dimensional model. Bound.-Layer Meteor., 18, 495–527, doi:10.1007/BF00119502.

Esterheld, J. M. and D. J. Giuliano, 2008: Discriminating between tornadic and non-tornadic supercells: A new hodograph technique. Electronic J. Severe Storms Meteor., **3** (2), 1–50.

Frame J. and Paul Markowski, 2010: Numerical Simulations of Radiative Cooling beneath the Anvils of Supercell Thunderstorms. *Mon. Wea. Rev.*, **138**, 3024–3047

Halbert, K. T., W. G. Blumberg, and P. T. Marsh, 2015: "SHARPpy: Fueling the Python Cult". Preprints, 5th Symposium on Advances in Modeling and Analysis Using Python, Phoenix AZ.

Jiménez, P., Jimy Dudhia, J. Fidel González-Rouco, Jorge Navarro, Juan P. Montávez, and Elena García-Bustamante, 2012: A Revised Scheme for the WRF Surface Layer Formulation. *Mon. Wea. Rev.*, **140**, 898–918.

Klemp, J., and Robert B. Wilhelmson, 1978: The Simulation of Three-Dimensional Convective Storm Dynamics. *J. Atmos. Sci.*, **35**, 1070–1096.

Kumjian, M., Zachary J. Lebo, and Hughbert C. Morrison, 2015: On the Mechanisms of Rain Formation in an Idealized Supercell Storm. *Mon. Wea. Rev.*, **143**, 2754–2773.

Mansell, E. R., C. L. Ziegler, and E. C. Bruning, 2010: Simulated electrification of a small thunderstorm with two-moment bulk microphysics. J. Atmos. Sci., **67**, 171-194.

Markowski, P., Christina Hannon, Jeff Frame, Elise Lancaster, Albert Pietrycha, Roger Edwards, and Richard L. Thompson, 2003: Characteristics of Vertical Wind Profiles near Supercells Obtained from the Rapid Update Cycle. *Wea. Forecasting*, **18**, 1262–1272.

Markowski, P., Yvette Richardson, James Marquis, Robert Davies-Jones, Joshua Wurman, Karen Kosiba, Paul Robinson, Erik Rasmussen, and David Dowell, 2012: The Pretornadic Phase of the Goshen County, Wyoming, Supercell of 5 June 2009 Intercepted by VORTEX2. Part II: Intensification of Low-Level Rotation. *Mon. Wea. Rev.*, **140**, 2916–2938.

Markowski, P., and Y. Richardson, 2014a: The Influence of Environmental Low-Level Shear and Cold Pools on Tornadogenesis: Insights from Idealized Simulations. *J. Atmos. Sci.*, **71**, 243–275.

Markowski, P., and Y. Richardson, 2014b: The origins of vortex sheets in a simulated supercell thunderstorm. *Mon. Wea. Rev.*, **142**, 3944–3954.

Markowski P., and Y. Richardson, 2014c: The Markowski and Richardson toy simulations revisited: what is the effect of surface drag?. 27th Conference on Severe Local Storms, Madison, Wisconsin.

Naylor, J., and Matthew S. Gilmore, 2012: Convective Initiation in an Idealized Cloud Model Using an Updraft Nudging Technique. *Mon. Wea. Rev.*, **140**, 3699–3705.

Nowotarski, C. and A. Jensen, 2014: Objective classification of supercell environments using multivariate self-organizing maps for research and forecasting. 27th Conference on Severe Local Storms, Madison, Wisconsin.

Nowotarski, C., Paul M. Markowski, Yvette P. Richardson, and George H. Bryan, 2015: Supercell Low-Level Mesocyclones in Simulations with a Sheared Convective Boundary Layer. *Mon. Wea. Rev.*, **143**, 272–297.

Parker, M., 2014: Composite VORTEX2 Supercell Environments from Near-Storm Soundings. *Mon. Wea. Rev.*, **142**, 508–529.

Parker M. and Johannes M. L. Dahl. (2015) Production of Near-Surface Vertical Vorticity by Idealized Downdrafts. *Monthly Weather Review* **143**:7, 2795-2816.

Rasmussen, E., J. Straka, Robert Davies-Jones, Charles A. Doswell III, Frederick H. Carr, Michael D. Eilts, and Donald R. MacGorman, 1994: Verification of the Origins of Rotation in Tornadoes Experiment: VORTEX. *Bull. Amer. Meteor. Soc.*, **75**, 995–1006.

Rasmussen, E. and D. Blanchard, 1998: A Baseline Climatology of Sounding-Derived Supercell and Tornado Forecast Parameters. *Wea. Forecasting*, **13**, 1148–1164.

Schenkman, A., Ming Xue, and Ming Hu, 2014: Tornadogenesis in a High-Resolution Simulation of the 8 May 2003 Oklahoma City Supercell. *J. Atmos. Sci.*, **71**, 130–154.

Shu, C. W. (2003). High-order finite difference and finite volume WENO schemes and discontinuous Galerkin methods for CFD. *International Journal of Computational Fluid Dynamics*, ***17***(2), 107-118.

Stull, R. B., 1988: An Introduction to Boundary Layer Meteorology. Kluwer Academic Publishers, 665 pp.

Thompson, R. Roger Edwards, John A. Hart, Kimberly L. Elmore, and Paul Markowski, 2003: Close Proximity Soundings within Supercell Environments Obtained from the Rapid Update Cycle. *Wea. Forecasting*, **18**, 1243–1261.

Thompson, R. Corey M. Mead, and Roger Edwards, 2007: Effective Storm-Relative Helicity and Bulk Shear in Supercell Thunderstorm Environments. *Wea. Forecasting*, **22**, 102–115.

Wicker, L., and William C. Skamarock, 2002: Time-Splitting Methods for Elastic Models Using Forward Time Schemes. *Mon. Wea. Rev.*, **130**, 2088–2097.

Wilhelmson, R., and Ching-Sen Chen, 1982: A Simulation of the Development of Successive Cells Along a Cold Outflow Boundary. *J. Atmos. Sci.*, **39**, 1466–1483.

Wurman J., David Dowell, Yvette Richardson, Paul Markowski, Erik Rasmussen, Donald Burgess, Louis Wicker, and Howard B. Bluestein, 2012: The Second Verification of the Origins of Rotation in Tornadoes Experiment: VORTEX2. *Bull. Amer. Meteor. Soc.*, **93**, 1147–1170.

Ziegler, C. L., 1985: Retrieval of thermal and microphysical variables in observed convective storms. Part I: Model development and preliminary testing. J. Atmos. Sci., **42**, 1487-1509.

Figures:

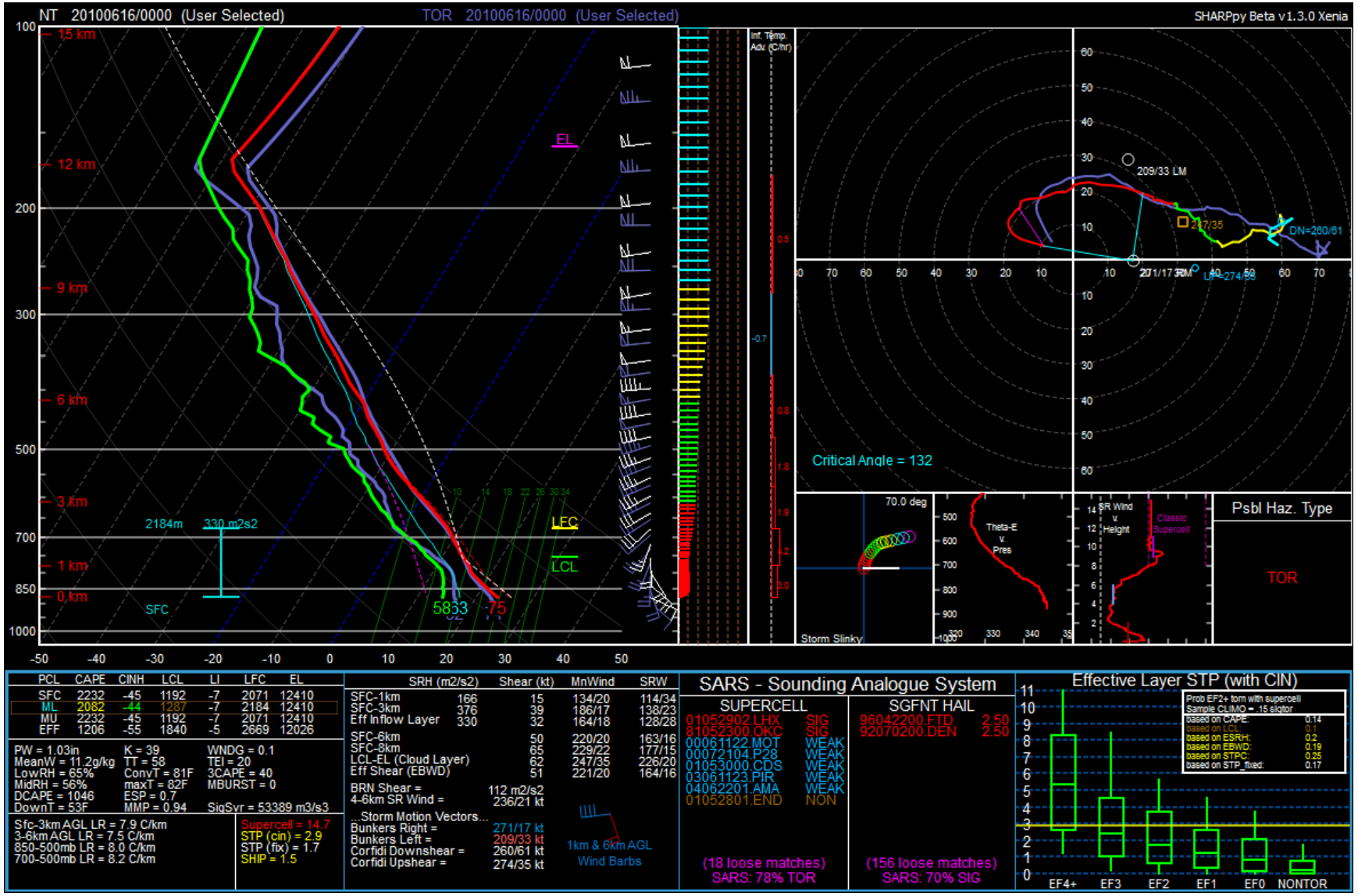

Figure 1: Skew-T log*P* diagram and hodograph showing the steady-state, non-tornadic VORTEX2 near-inflow composite sounding. The tornadic profile is shown in purple. Plotted using SHARPpy (Kelton et al. 2015).

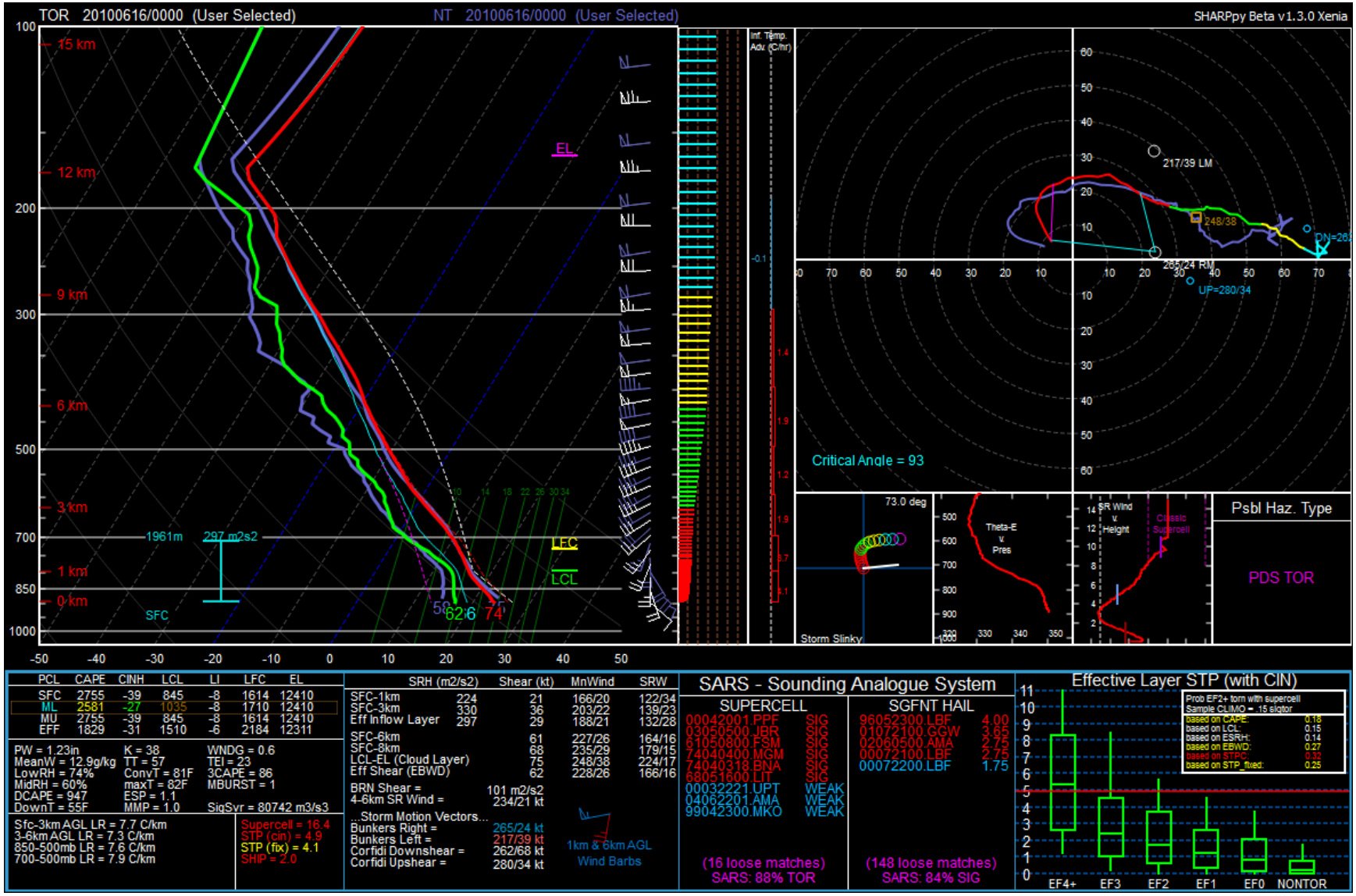

Figure 2: As in Figure 1, except for the steady-state, tornadic VORTEX2 near-inflow composite sounding. The non-tornadic profile is shown in purple.

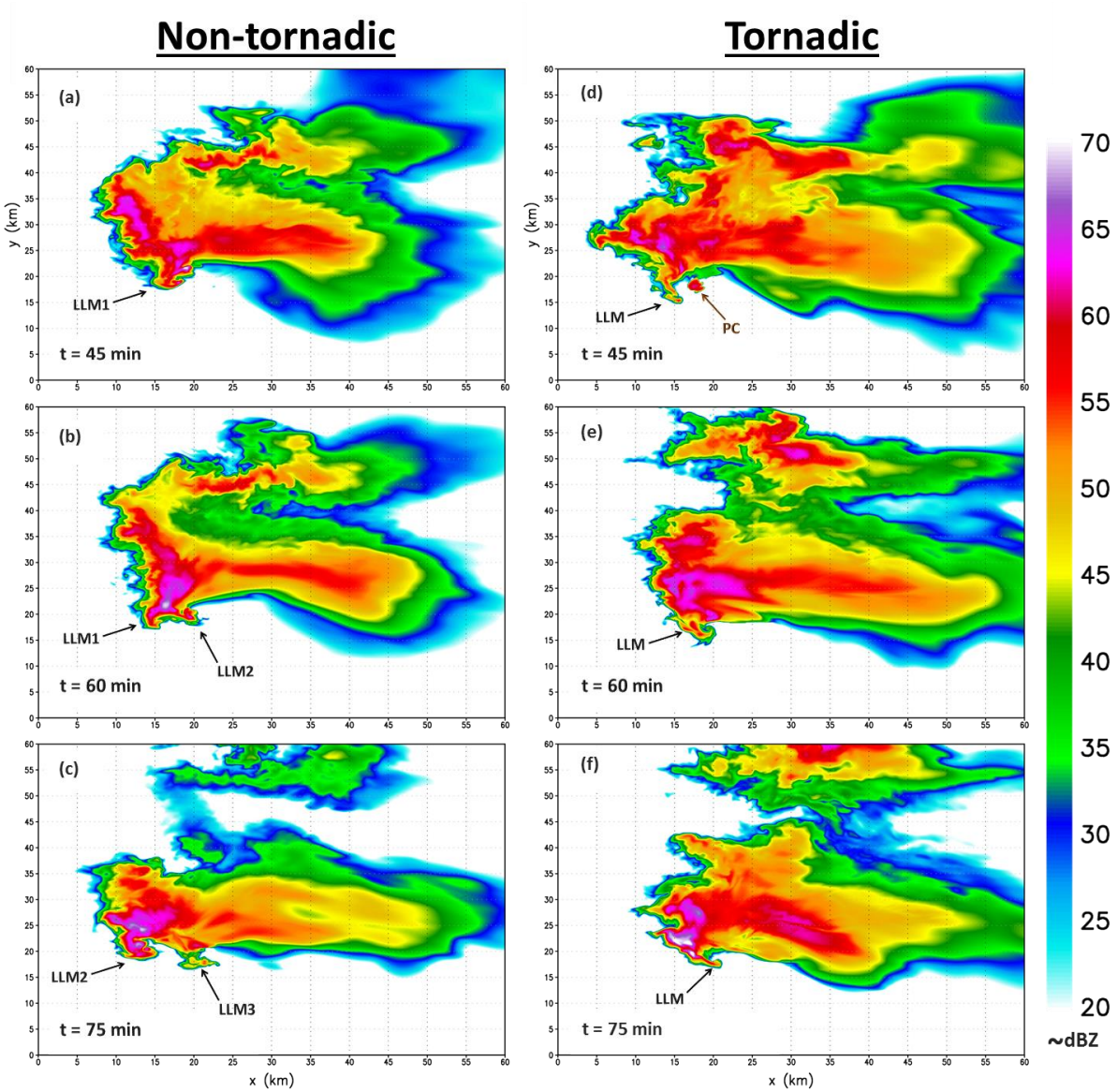

Figure 3: Model-simulated reflectivity at 10 m for (left) the non-tornadic supercell and (right) the tornadic supercell. Various low-level mesocyclones (LLM) are annotated. The developing precipitation curtain is annotated in panel d.

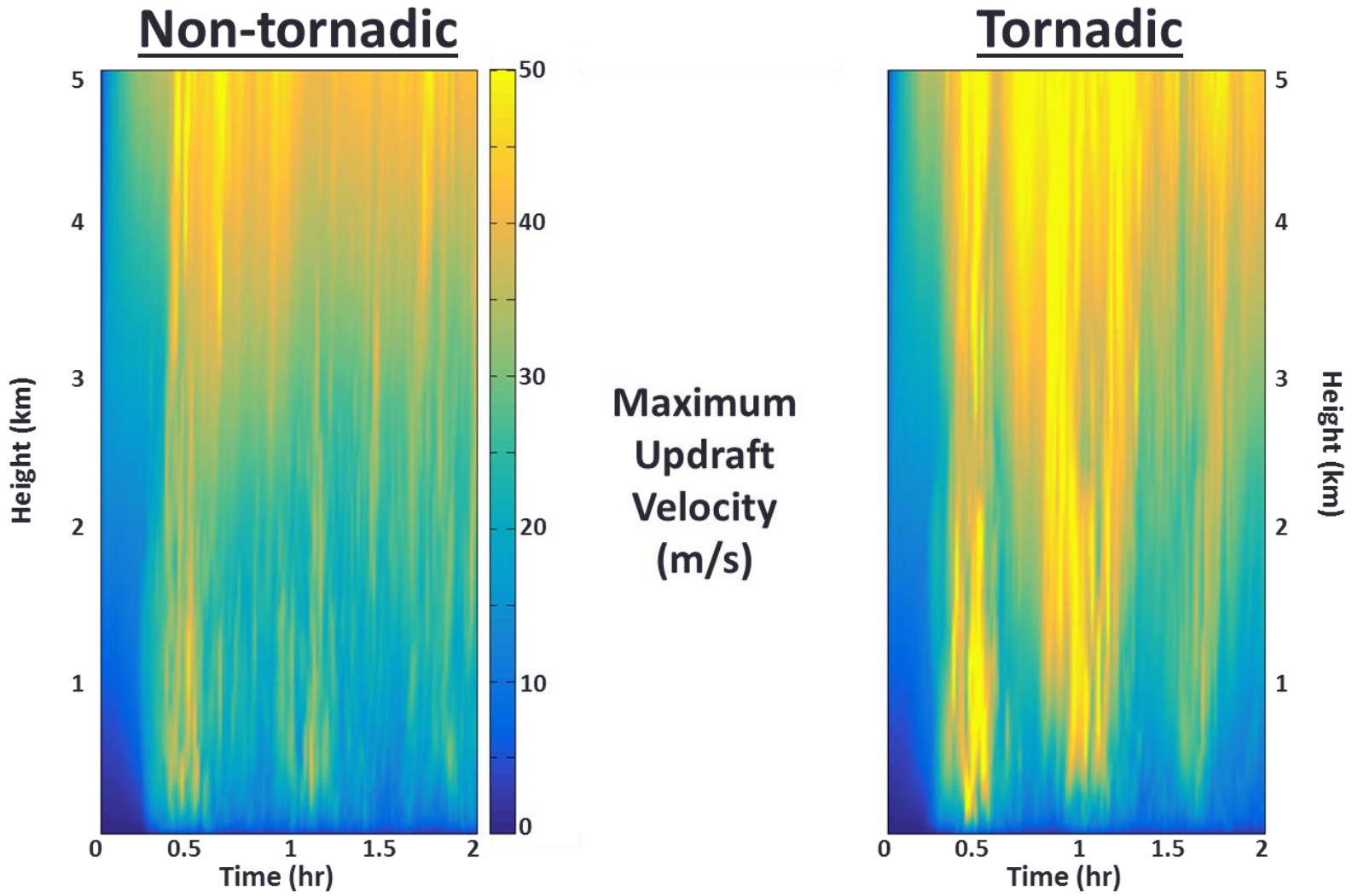

Figure 4: Time–height plot of the maximum vertical vorticity (s^{-1}) in a 50 km x 50 km box following the supercells' mesocyclone for (left) the non-tornadic supercell and (right) the tornadic supercell.

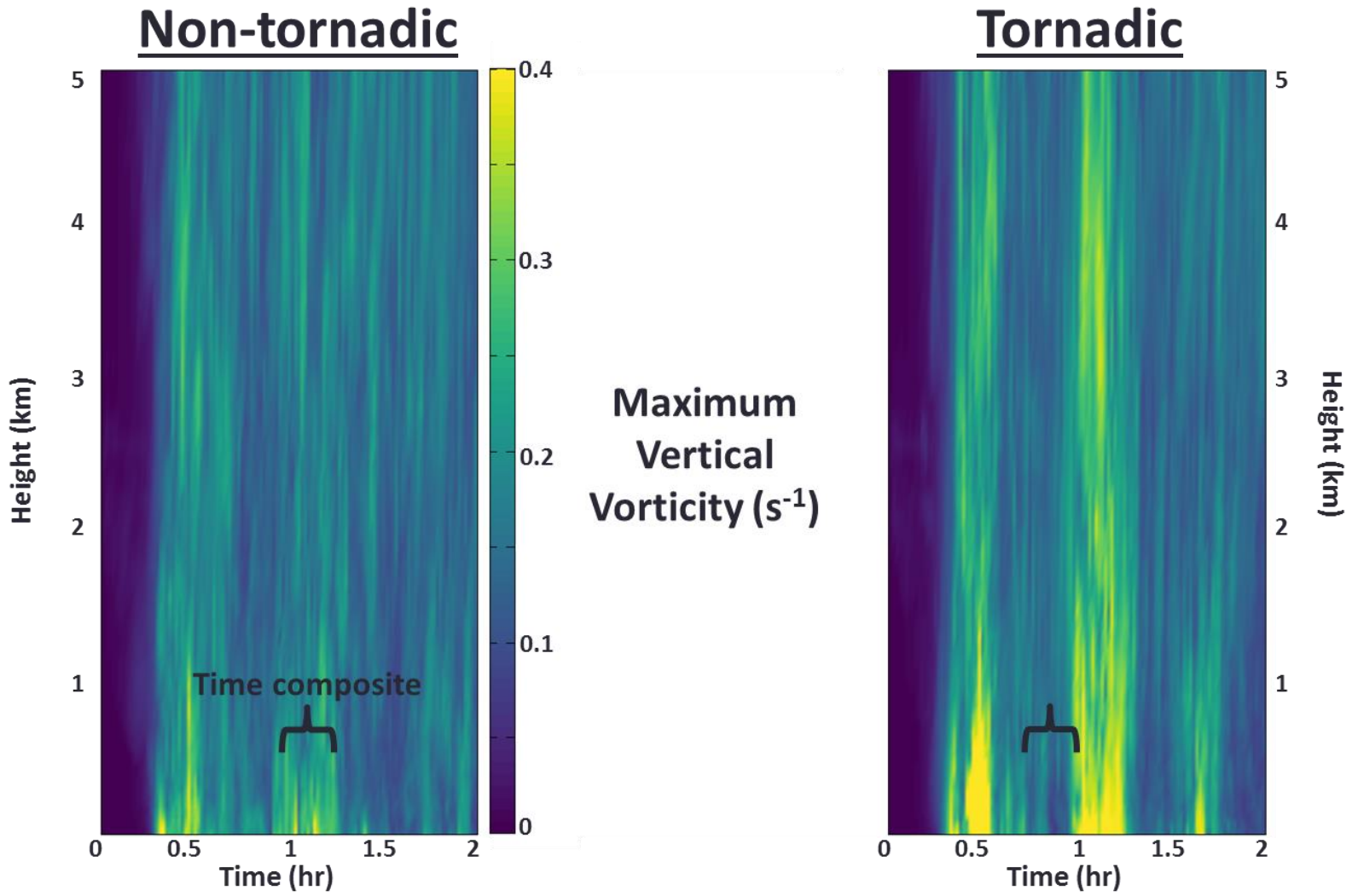

Figure 5: As in Figure 4, but for the maximum vertical velocity (m/s). The 15 minute time composite period for Figure 6 are annotated for each simulation.

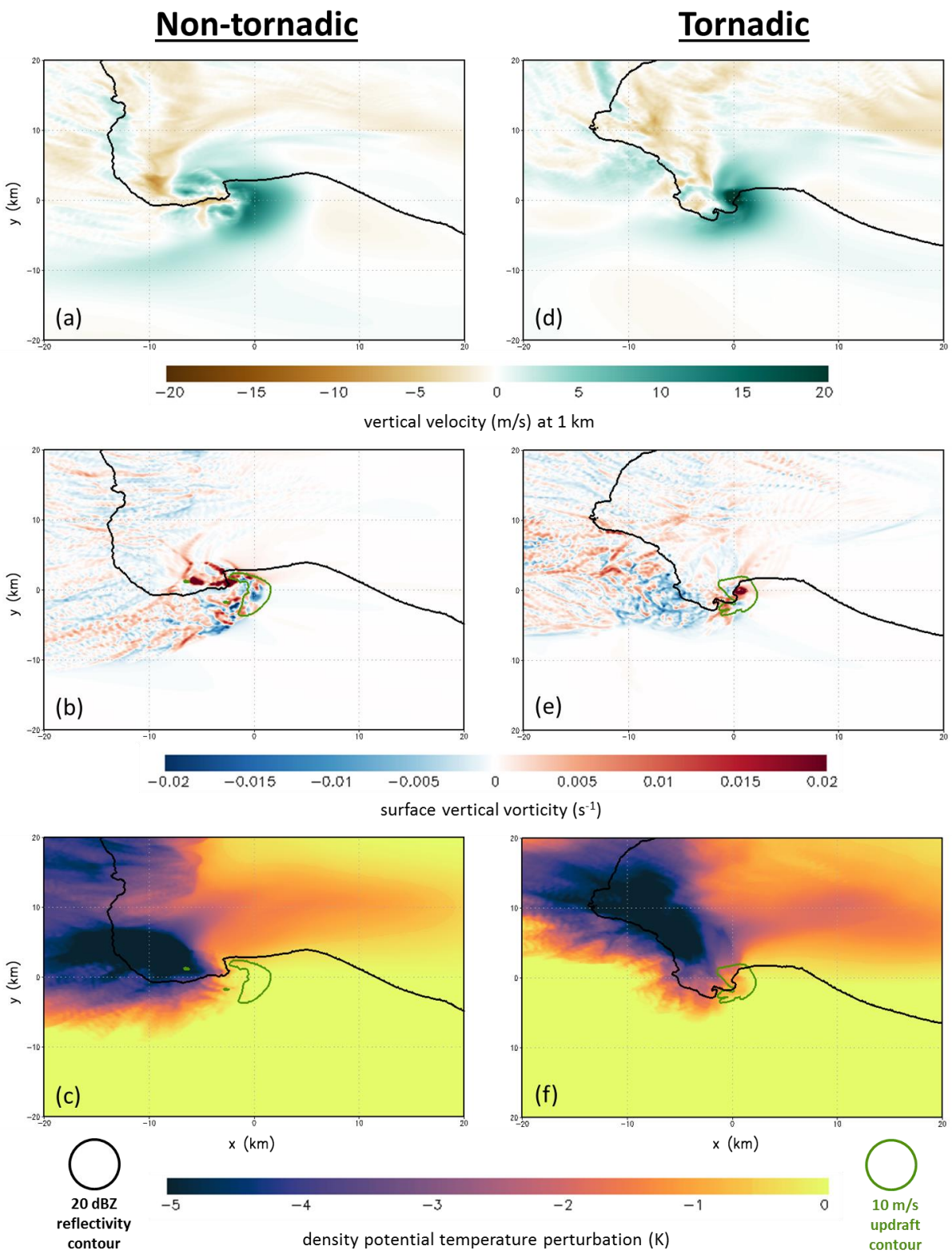

Figure 6: Time composite plot showing the average spatial (top) 1-km vertical velocity field (m/s), (middle) 10 m vertical vorticity field (s^{-1}), and (bottom) 10 m density potential temperature deficit (K) for (left) the non-tornadic supercell and (right) the tornadic supercell.

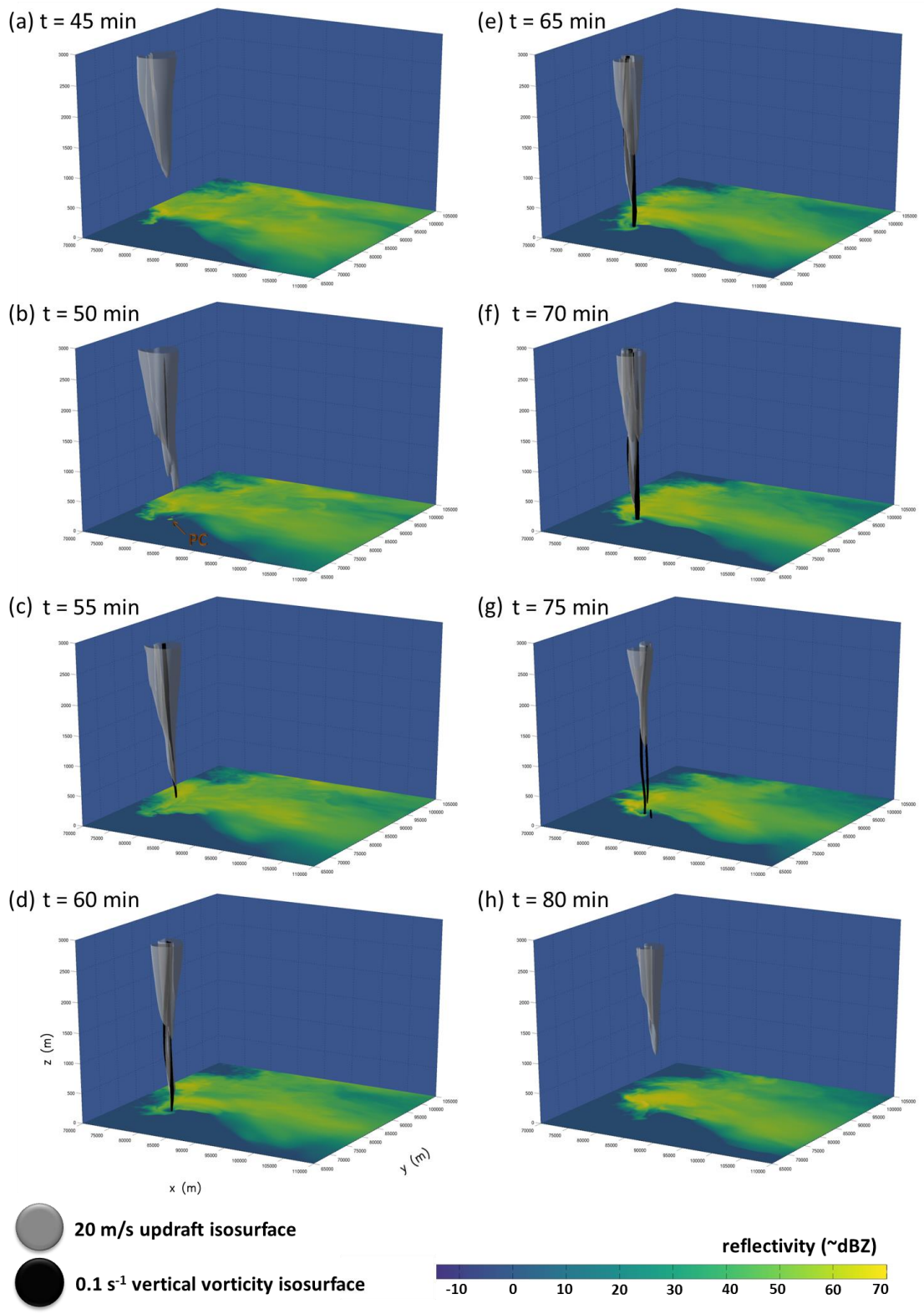

Figure 7: Three-dimensional view of the low-level updraft and vertical vorticity and the 10 m reflectivity field for the tornadic supercell. Shaded on the surface is the model-simulated base reflectivity (~dBZ). Updraft and vertical vorticity isosurfaces of 20 m/s and 0.1 s^{-1} is shown light gray and black, respectively. The developing precipitation curtain is annotated in panel b.

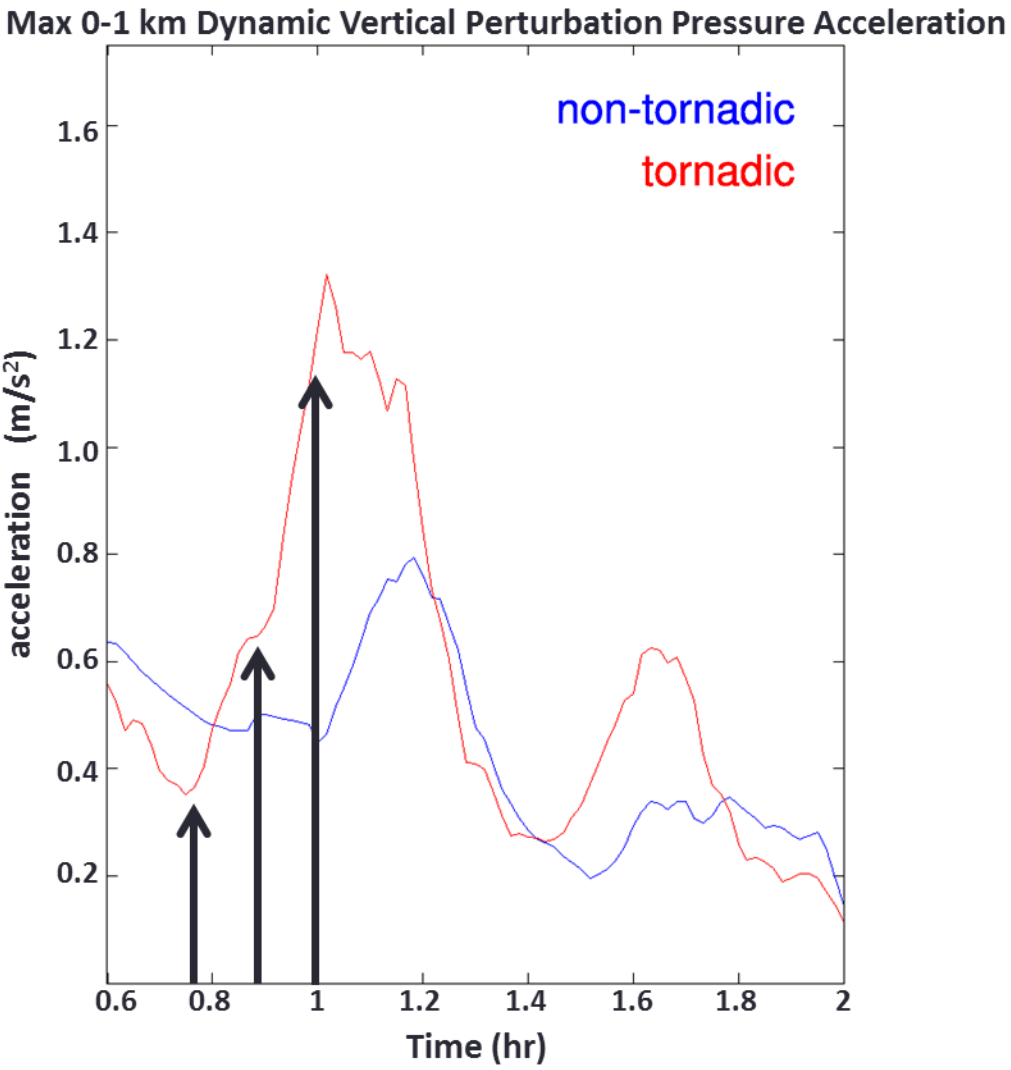

Figure 8: Time series comparing the dynamic vertical perturbation pressure gradient acceleration (VPPGA; m/s^2) for both the non-tornadic supercell (blue) and the tornadic supercell (red). Black arrows roughly refer to same time as shown in Fig. 7 panels a, c, d.

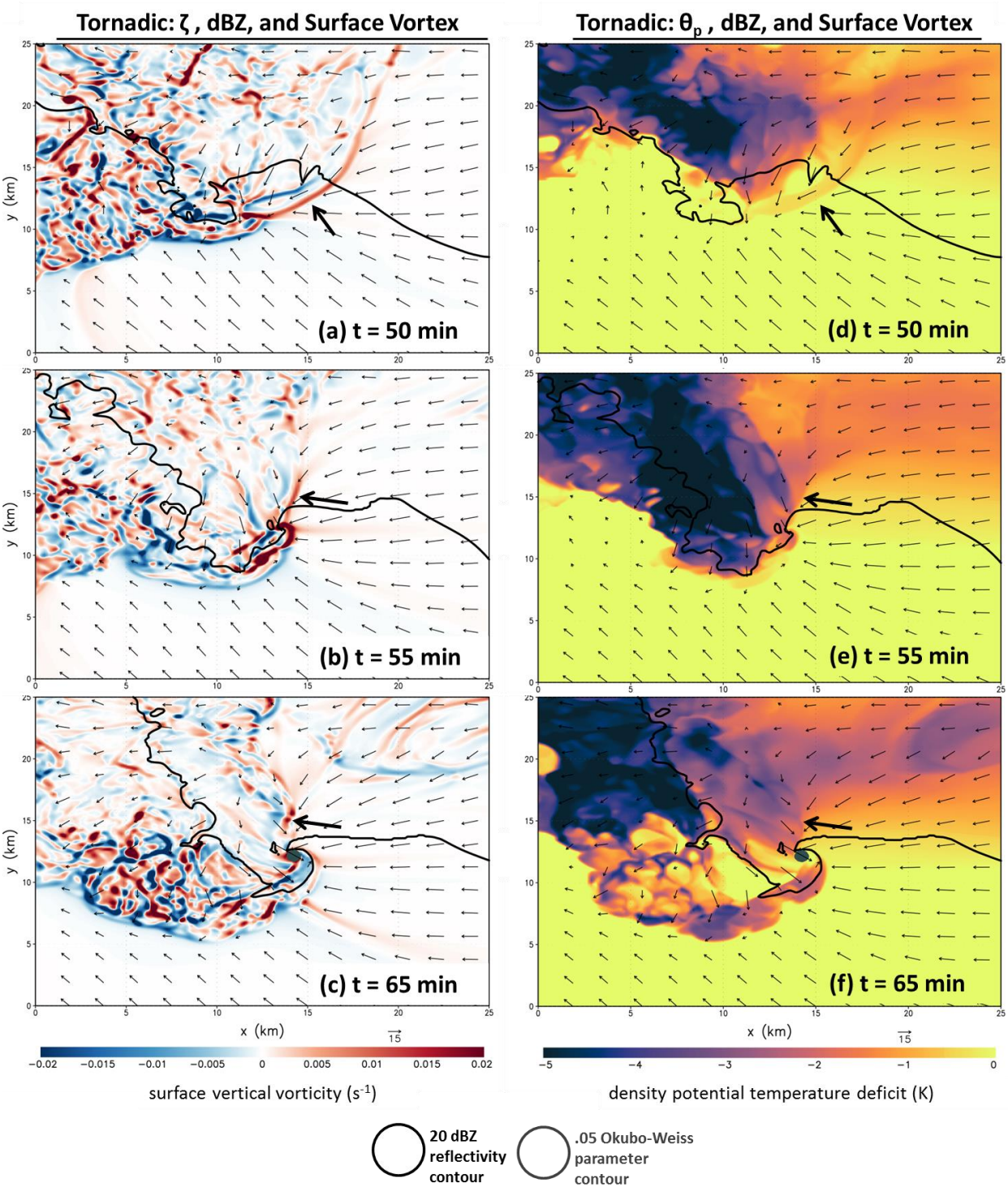

Figure 9: Model-simulated (left) 10 m vertical vorticity (s^{-1}) and (right) 10 m density potential temperature deficit (K) for the tornadic supercell. The forward flank vortex sheet is annotated in panels a,d. The vorticity river is annotated in panels b-c, e-f.